Applied Radiation and Isotopes 170 (2021) 109598

Contents lists available at ScienceDirect

Applied Radiation and Isotopes

journal homepage: http://www.elsevier.com/locate/apradiso

Evaluation of high-linearity bone radiation detectors exposed to gamma-rays via FTIR measurements

Lucas Nonato de Oliveira [a,b,*], Eriberto Oliveira do Nascimento [a], Pedro de Aquino Morais Júnior [a], Patrícia de Lara Antonio [b], Linda V.E. Caldas [b]

[a] Instituto Federal de Educação, Ciência e Tecnologia de Goiás-IFG, Rua 75 No 46, 74055-110, Goiânia, GO, Brazil
[b] Instituto de Pesquisas Energéticas e Nucleares, Comissão Nacional de Energia Nuclear-IPEN/CNEN, Av. Prof. Lineu Prestes2242, 05508-000, São Paulo, SP, Brazil

ARTICLE INFO

Keywords:
Bone
Radiation dosimetry
PLSR and PCR analyses
FTIR technique
High doses

ABSTRACT

In radiation physics, the study of new alternative dosimeters is of interest to the growing branch of dosimetric characterization for radiotherapy applications. The goal of this work was to expose bone samples to high doses and evaluate their linearity response to gamma rays. The Fourier Transform Infrared (FTIR) spectrophotometry technique was employed as the evaluation technique, and based on the spectrophotometry absorbance profiles the linearity was assessed based on the following methods: Area Under the Curve (AUC), Wavenumber Method (WM), Partial Component Regression (PCR) and Partial Least-Square Regression (PLSR) methods. The bone samples were irradiated with absorbed doses of 10 Gy up to 500 Gy using a ^{60}Co Gamma Cell-220 system. The results showed, for the calibration curves of the system, adequate linearity on all methods. In conclusion, the results indicate a good linear response and therefore an interesting potential radiation detector.

1. Introduction

Gamma irradiation applied to bone has been investigated in recent years (Bargh et al., 2020; Bonet et al., 2020; Drost et al., 2017; Kazakis and Tsirliganis, 2019; Shiloh and Krishnan, 2018; Sung and Choi, 2015). It is known that gamma irradiation causes damage to bones physically, chemically and structurally, and that spectroscopy is a technique used to evaluate irradiated bones (Bayarı et al., 2020; Chaber et al., 2017; Kontopoulos et al., 2018; Kubisz and Połomska, 2007; Rudko et al., 2009). Dosimetric information on bone irradiations has recently been investigated, bringing useful results regarding the absorbed dose in media adjacent of the bone and in its depth (Saleh et al., 2021).

The radiation-induced change in bone composition has been studied (Mandair et al., 2020; Govey et al., 2016). For biodosimetry, this effect causes changes in the material under analysis, in which the absorbed dose in the radiobiological material can be evaluated (Baker et al., 2014). For good accuracy of the absorbed dose rate, some methods for reducing the noise signal (SNR) are seen in the equipment that shows the response assessment with extended measurement times (Harig, 2004; Tiplady et al., 2019). The SNR can be minimized with some strategies such as: increasing the sample measurement time, which can reduce random errors, sample format which can have a non-linear interference caused by the matrix composition, or even the quality of the equipment (due to the evolution of its electronic components) (Rogalski, 2002).

Since bone is a solid-state material, a relationship can be established with some solid-state dosimeters to evaluate a linear response for dosimeters; with that, many applications can emerge in medical physics. Therefore, if bone samples manifest a linear response, they may be applied as candidates for use as linear dosimeters (de Oliveira et al., 2014; Lu et al., 2020; Musto et al., 2019; Parwaie et al., 2020; Polanek et al., 2020).

In this way, there are some methods already defined in the literature that seek to evaluate the linearity and sensitivity of a given dosimeter. Those are the "wavelength" and "under the curve" methods (de Oliveira et al., 2019), here and forth writing they as WM and AUC methods. These methods provide a quick response, due to their operational convenience, and guarantee on the linearity over spectra from FTIR measurements.

Statistical analyses such as Partial Component Regression (PCR) and Partial Least-Square Regression (PLSR) have already been used elsewhere (Das et al., 2020; dos Santos et al., 2020; Helland, 2001; Jiang and Lu, 2018; Urbański, 1994; Zhang et al., 2017). In this case, they can be useful in the investigation of dosimetric characteristics, where a high degree of multicollinearity is presented. A summary of PCR and PLSR:

* Corresponding author. Instituto Federal de Educação, Ciência e Tecnologia de Goiás-IFG, Rua 75 No 46, 74055-110, Goiânia, GO, Brazil.
E-mail address: lucas@ifg.edu.br (L. Nonato de Oliveira).

https://doi.org/10.1016/j.apradiso.2021.109598
Received 23 September 2020; Received in revised form 19 December 2020; Accepted 13 January 2021
Available online 29 January 2021
0969-8043/© 2021 Elsevier Ltd. All rights reserved.

Table 1
Correlation matrix for bone sample irradiated with gamma rays and absorbed doses of 10 Gy, 100 Gy, 250 Gy, 400 Gy and 500 Gy and absorbance averages.

Absorbance average	Absorbed dose	10 Gy	100 Gy	250 Gy	400 Gy	500 Gy
0.0111	10 Gy	1.0000				
0.0173	100 Gy	0.9880	1.0000			
0.0457	250 Gy	0.9835	0.9926	1.0000		
0.0478	400 Gy	0.9693	0.9823	0.9945	1.0000	
0.0746	500 Gy	0.9776	0.9901	0.9995	0.9956	1.0000

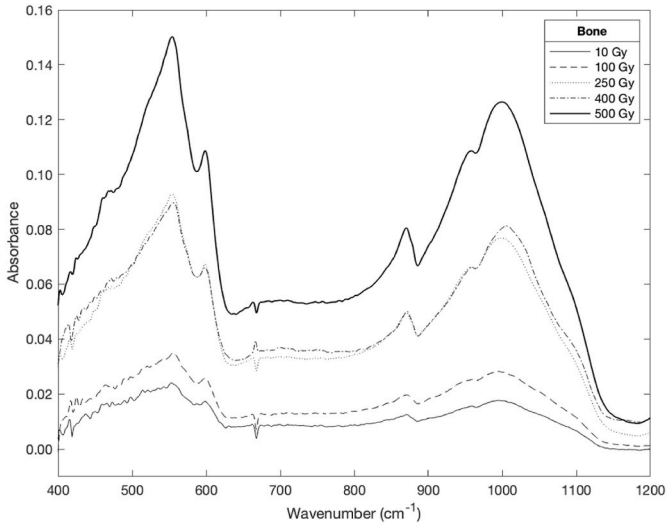

Fig. 1. FTIR spectra, absorbance *versus* wavenumber, for bone samples irradiated with absorbed doses from 10 Gy to 500Gy (^{60}Co source). The average of 3 samples was evaluated for each curve, and the uncertainty obtained was lower than 1%. The uncertainty was of type C, which considers the root sum squared (RSS) of the uncertainties A (from measurements) and the uncertainties B (from equipment).

the first one makes the regression relating the data especially of X and then with Y, and the second one makes the regression relating simultaneously X and Y data (Li et al., 2020; Luinge et al., 1995).

This work aimed to investigate the effect of gamma radiation in biological calcified tissue samples for their linearity response using the area under the curve (AUC) and wavenumber (WM) methods, and comparison with PCR and PLSR traditional approach methods, and the FTIR spectrophotometry technique for biodosimetry. Besides that, using the WM, the dosimeter sensitivity regarding the absorbed dose was evaluated.

2. Materials and methods

Small cubes with size approximately of 0.125 cm^3 composed the bone samples, used in this work. This material was made with the bovine femur part, and each bone cube was cut with the diamond technique so that they all got the same dimensions; the average slaughter weight in Brazil is 18 arrobas, which is equivalent to an age from 9 months to 14 months; this age is important for measurements that use the FTIR technique (Petra et al., 2005). The samples were irradiated in triplicates, with absorbed doses of 10 Gy, 100 Gy, 250 Gy, 400 Gy and 500 Gy using a ^{60}Co Gamma Cell-220 system (dose rate of 1.089 kGy/h at the Radiation Technology Center of IPEN); afterwards, the absorbance spectrum of each sample was acquired on a Fourier Transform Infrared (FTIR) Spectrometer (Frontier/PerkinElmer) from 400 cm^{-1} to 1200 cm^{-1}, with 1 cm^{-1} spectral resolution.

Four spectrophotometric methods were used to study the linearity response for the irradiated bone samples, as follows:

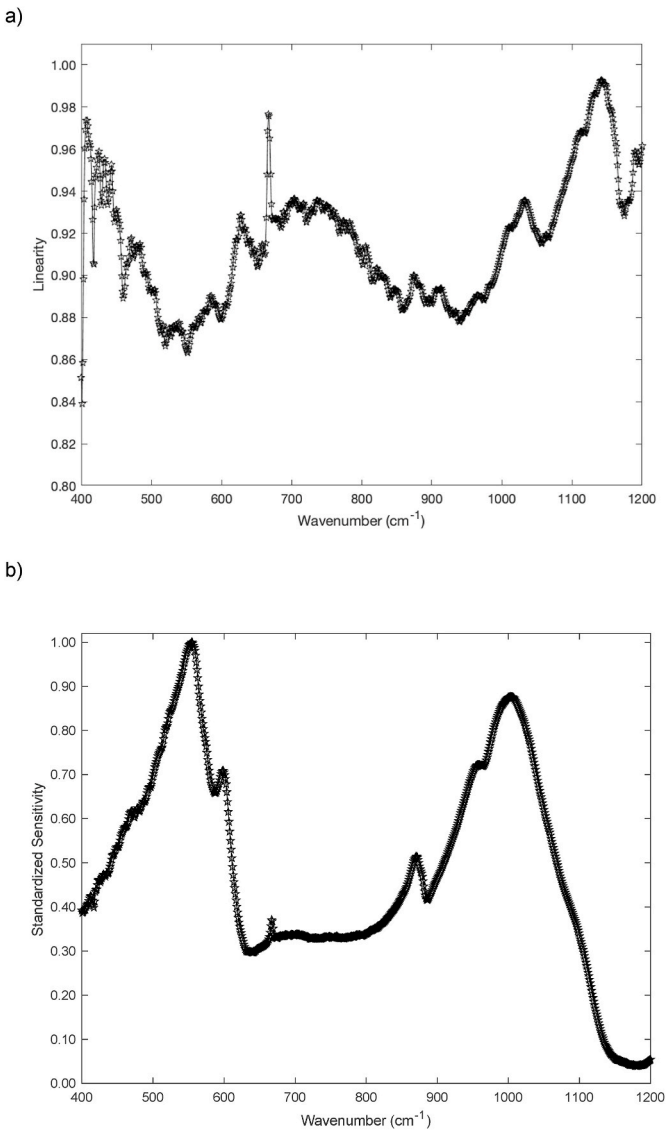

Fig. 2. a) Linearity *versus* wavenumber and b) Normalized sensitivity *versus* wavenumber.

AUC: The area under each absorbance spectrum is calculated, then the area was assigned respectively to its corresponding absorbed dose, which varied discretely: 10 Gy, 100 Gy, 250 Gy, 400 Gy and 500 Gy. Subsequently, a linear regression was evaluated, using as predictive variable the absorbed dose, and the response variable was set as the area under the curve. The linearity was evaluated using the squared Pearson correlation coefficient (R^2).

WM: In this method, all absorbance spectra are evaluated iteratively. To illustrate, given a fixed wavenumber, the respective absorbance values are searched in each different spectrum corresponding to the following absorbed doses of 10 Gy, 100 Gy, 250 Gy, 400 Gy and 500 Gy. At the end, the absorbed doses and the respective absorbances are stored as functions of the wavenumber index. Then, the linear regression is performed considering as independent variables the absorbed doses and as predictive variables, the absorbance values gathered from each spectrum. Linearity is then evaluated considering squared Pearson correlation coefficient. This process is repeated for each wavenumber until scanning the entire spectrum from 400 cm^{-1} to 1200 cm^{-1}. To evaluate globally the WM results regarding the linearity given by the R^2 value, the Cumulative distribution function (CDF) was employed.

For the PCR and PLSR methods, the $X_{n\times m}$ matrix contains the m

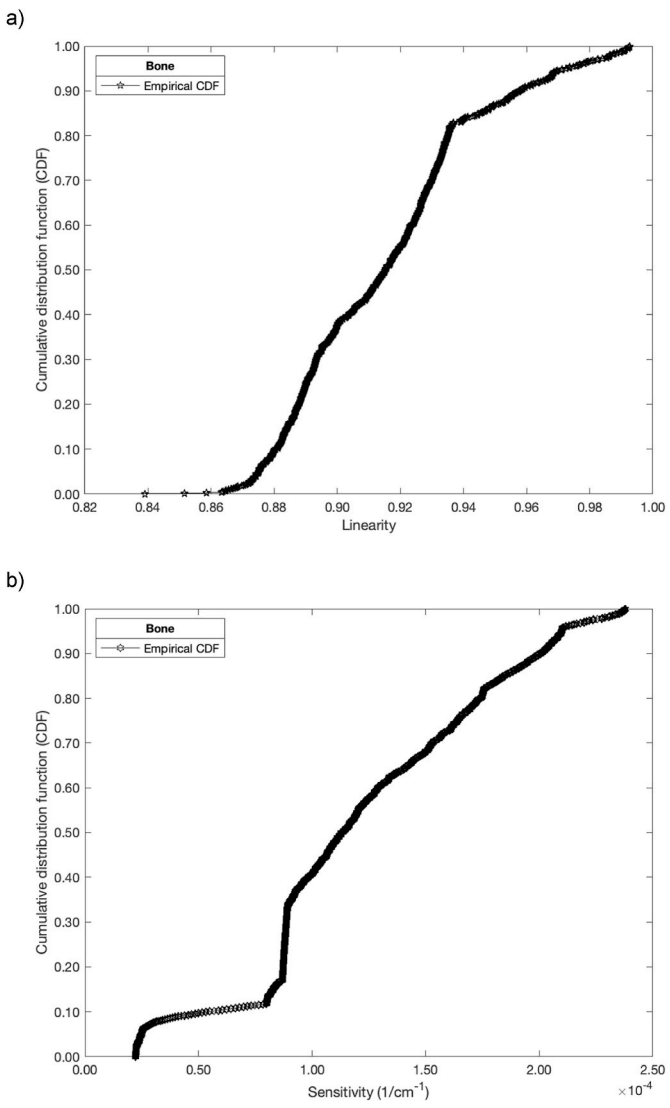

Fig. 3. a) Cumulative distribution function (CDF) *versus* linearity and b) Cumulative distribution function (CDF) *versus* sensitivity.

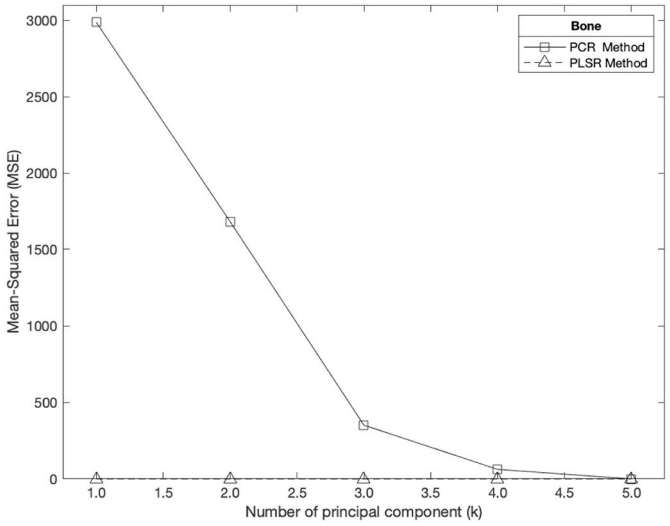

Fig. 4. Mean-squared error (MSE) *versus* number of principal components (PC) for PCR and PLSR methods.

absorbance values indexed according to the spectrum from 400 cm^{-1} to 1200 cm^{-1}, these values are the regressor variables in relation to the n absorbed doses that correspond to the observations. The absorbed doses were assigned by the $y_{n\times1}$ row vector. The PCR algorithm is given as:

i) Initialize with $X_{n\times m}$ and $y_{n\times1}$ data, for $m = 800$ and $n = 5$ that are numbers of regressors and observations, respectively:

$$X_{n\times m} = \begin{bmatrix} x_{11} & \cdots & x_{1m} \\ \vdots & \ddots & \vdots \\ x_{n1} & \cdots & x_{nm} \end{bmatrix},\ y_{n\times1} = \begin{bmatrix} y_1 \\ \vdots \\ y_n \end{bmatrix}$$

ii) Calculate the mean-centered data matrix of X (the values for each column are obtained subtracting their respective averages), called now X_C

$$X_C = \left(I - \frac{1}{n}11'\right)X$$

In the expanded matrix form, X_C is written as:

$$X_C = \begin{bmatrix} \left(x_{11} - \overline{x}_1\right) & \cdots & \left(x_{1m} - \overline{x}_m\right) \\ \vdots & \ddots & \vdots \\ \left(x_{n1} - \overline{x}_1\right) & \cdots & \left(x_{nm} - \overline{x}_m\right) \end{bmatrix} = \begin{bmatrix} x_{C11} & \cdots & x_{C1m} \\ \vdots & \ddots & \vdots \\ x_{Cn1} & \cdots & x_{Cnm} \end{bmatrix}$$

iii) From the eigensystem $X_C{}'X_C$, calculate the eigenvectors (A) and eigenvalues (Λ). The trace of the Λ matrix are the eigenvalues expressed in the vector form $\lambda_{mx1}\Lambda = \begin{bmatrix} \lambda_{11} & 0 & 0 \\ 0 & \lambda_{22} & 0 \\ 0 & 0 & \lambda_{mm} \end{bmatrix}$,

$[A_{m\times m}\ \lambda_{m\times1}] = \mathrm{EVD}(X_C{}'X_C)_{m\times m}$

iv) Sort eigenvalues in descending order and rearrange the eigenvectors according to sorted order;

v) Verify if A is an orthonormal matrix cheking the trueness of the following relation:

$$A_{m\times m}A'_{m\times m} = I_{m\times m}$$

vi) Obtain the Z matrix, from X_C and A;

$$Z_{n\times m} = X_{C_{n\times m}}A_{m\times m}$$

At this moment, seeking to avoid the multicollinearity effects, deflate the Z matrix by choosing 1 up to 5 for the optimal number of principal components (k) that Z can have.

$$Z_{n\times k} = X_{C_{n\times m}}A_{m\times k}$$

vii) Calculate the regression coefficient estimator (γ) in accordance to the deflation made in step vi;

$$\gamma_{k\times1} = \left(Z^TZ\right)^{-1}Z'y = Z'_{k\times k}Z_{k\times n}y_{n\times1}$$

viii) Finally, obtain the PCR estimates of y, named as $y_{PCR_{n\times1}}$:

$$y_{PCR_{n\times1}} = Z_{n\times k}\gamma_{k\times1}$$

In the PCR algorithm: $(.)'$, $(.)^{-1}$, I_m, 1_n and EVD are transpose matrix operator, inverse matrix operator, identity matrix of order m, a square matrix filled with ones of order n and the Eigenvalue Decomposition (EVD) operator, respectively.

The PLSR algorithm can be found in detail in the literature (Wold et al., 2001). In PLSR pre-processing, the X data were normalized by mean-centering and adjusted by the standard deviation. The multivariate analysis was done in Matlab (2020a) (The MathWorks Ins., Natick, USA).

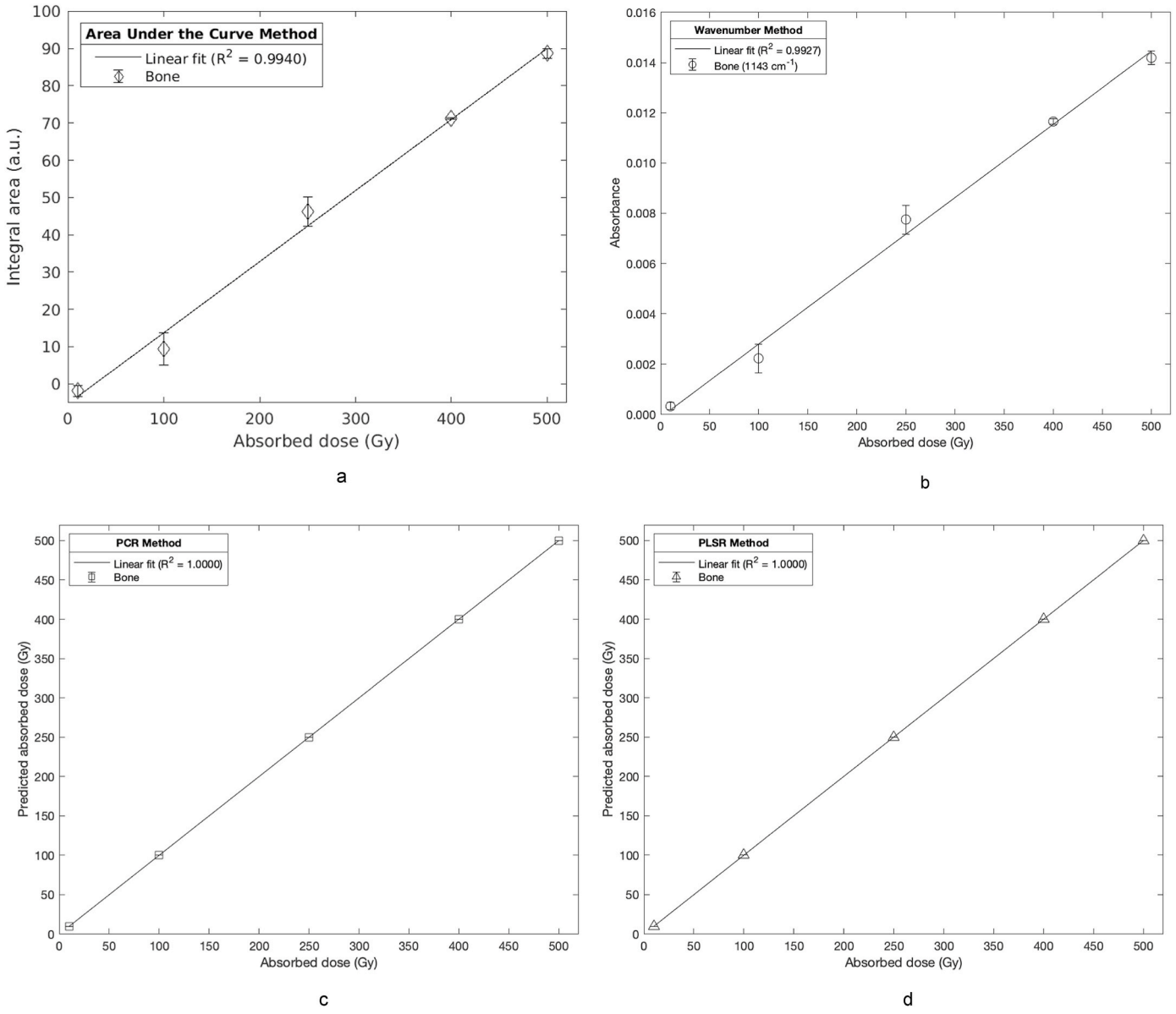

Fig. 5. Calibration curves for AUC, WM, PCR and PLSR methods. a) Integral area *versus* absorbed dose, b) Absorbance *versus* absorbed dose, c) Predicted absorbed dose *versus* absorbed dose and d) Predicted absorbed dose *versus* absorbed dose. The error bar represents, in the cases of the PCR and PLSR methods, the difference between the absorbed doses and the predicted absorbed doses. For the AUC methods, the error bar represents the difference between the points referring to the areas and the points coming from the linear fit. For the WM method, the error bar represents the difference between the maximum absorbance points and the linear fitted points.

The bone sample sensitivities in ($1/cm^{-1}$) were obtained applying the WM. Accordingly, a linear regression was performed between the absorbed doses and absorbance values at a given wavenumber. Seeking to enhance the relative sensitivity interpretation among all wavenumbers, a normalization process was employed, according to Eq. (1):

$$S(k) = \frac{m(k) - min(m)}{max(m) - min(m)} \tag{1}$$

where $S(k)$ is the normalized sensitivity at the wavenumber k, m is the sensitivity, $min(m)$ and $max(m)$ are the maximum and minimum sensitivities, respectively. The wavenumber, k, varied from 400 cm^{-1} to 1200 cm^{-1}, with 1 cm^{-1} spectral resolution.

The Mean Squared Error (MSE) was used to calculate the prediction accuracy (Bertrand et al., 2001) of the PCR and PLSR methods, given by Eq. (2):

$$MSE = \frac{1}{n}\sum_{i=1}^{n}\left(y_i - \widehat{y}_i\right)^2 \tag{2}$$

where $\widehat{y}_i$ is the absorbed dose prediction to the i^{th} value of the PCR or PLSR result, y_i is the actual absorbed dose for bone samples and n is the number of absorbed doses.

The residual values for AUC and WM were calculated by subtracting the expected independent variable value respective to the prediction value made by the linear regression according to each method. The expected independent variable value for the AUC was the area, and for the WM it was the absorbance values from a fixed wavenumber and for the WM. The residual values for the PCR and PLSR are defined as the difference between y_i and $\widehat{y}_i$, where $\widehat{y}_i$ can assume the prediction for the PCR given by y_{PCR} and PLSR as y_{PLSR}.

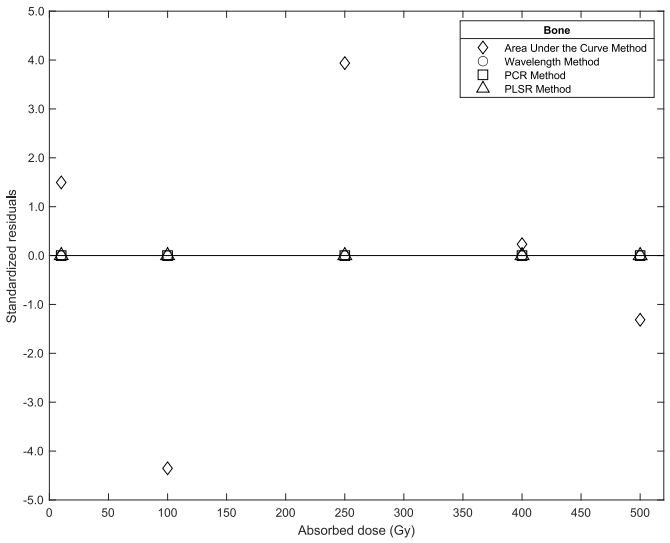

Fig. 6. Residuals versus absorbed dose for AUC, WM, PCR and PLSR methods applied to the bone samples.

3. Results and discussion

Table 1 shows the correlation matrix for the bone samples irradiated with gamma rays for all absorbed doses. In this table, the values for the correlation were greater than 0.9693, indicating a strong linear relationship. The p-values were <0.01, indicating that the absorbance averages are statistically different, as expected since with the increase in the absorbed dose an increase in absorbance values was observed. The results of the correlation matrix generated a high degree of collinearity, that is, it is possible to apply regression methods without loss of information from the measurements, with the use of methods that use all the information such as the PCR and PLSR methods.

Fig. 1 shows FTIR spectra, absorbance *versus* wavenumber, for bone samples irradiated with absorbed doses from 10 Gy to 500 Gy (^{60}Co source). The FTIR technique is simple and fast, and it allows to observe how the bone behaves when irradiated; another detail is that the bone does not change color with the administered absorbed doses. It is important to note that results like those obtained can be considered unique, since FTIR analyses depend on a series of factors such as reported in the literature: different particle size powder fraction (Kontopoulos et al., 2018); differences in chemical composition between the depth and surface can occur in the same tissue (Donnelly et al., 2012; Khanarian et al., 2014), or between different individuals and animals (Bachmann et al., 2003).

Results about linearity *versus* wavenumber and normalized sensitivity *versus* wavenumber are shown in Fig. 2a and b, respectively. For linearity, the maximum value of R^2 is 0.9927 for the wavenumber of 1143 cm^{-1}, and for regions between 1141 cm^{-1} and 1144 cm^{-1}; the other higher values of R^2 are between 0.9921 and 0.9926, respectively. For the normalized sensitivity, the maximum value is 1.0000 for the wavenumber of 556 cm^{-1}, and for regions between 553 cm^{-1} and 557 cm^{-1}; the other higher values are between 0.9947 and 0.9987, respectively. The values of maximum linearity and maximum normalized sensitivity have practically minimum values, 0.8698 and 0.0324 respectively, that is, the region of maximum linearity presents the minimum of sensitivity and the opposite is also true.

Fig. 3a and b shows the cumulative distribution function (CDF) *versus* linearity and cumulative distribution function *versus* sensitivity, respectively. For values between 0.80 and 1.00 to CDF, the values are: 0.9353 and 0.9927; and $1.73.10^{-4}$ and $2.37.10^{-4}$ for linearity and sensitivity, respectively. CDF increases faster for linearity than for normalized sensitivity.

The results for the Mean Squared Error (MSE) *versus* number of principal components for PCR and PLSR methods are shown in Fig. 4. In this figure, it can be observed that with the increase in the number of principal components (PC) the MSE decreased for the PCR method; for the PLSR method this value is zero for all PC.

In Fig. 5 are presented the calibration curves for AUC, WM, PCR and PLSR methods. Fig. 5a shows the integral area *versus* absorbed dose, Fig. 5b the absorbance *versus* absorbed dose, Fig. 5c the predicted absorbed dose *versus* absorbed dose for the PCR method, and Fig. 5d the predicted absorbed dose *versus* absorbed dose for the PLSR method. All four methods showed that they may be used in the search for linearity for irradiated bone; the maximum R^2 values were: 0.9340; 0.9927; 1.0000; 1.0000, for AUC, WM for the best 1143 cm^{-1} value of wavenumber, PCR and PLSR methods respectively. Although the maximum value of R^2 is 1.0000 for the PCR and PLSR methods, the latter has null MSE, which is considered the best method to determine linearity.

Fig. 6 presents the residuals versus absorbed dose for AUC, WM, PCR and PLSR methods applied to the bone samples.

The method with the greatest residual error (−7.6737) is the AUC method, followed by the WM method with 0.6% residual error, the other PCR and PLSR methods presented null residual errors. In this scenario, the PLSR method is considered the best method for analyzing the linearity for irradiated bone samples in addition to having MSE and residual equal to zero.

4. Conclusions

For the samples of irradiated bone, the following final aspects are observed: i) FTIR spectrophotometry is a technique that may be used in measurements of irradiated bones; ii) the methods can be used to find the linearity according to the need and precision of the work; iii) in terms of linearity, the best methods in order were: PLSR, PCR, AUC and WM. In conclusion, the results of bone samples indicate an acceptable linear response in function of absorbed dose, and therefore this material presents a potential use as a radiation detector.

Credit author contribution statement

Lucas Nonato de Oliveira: Conceptualization, Methodology, Validation, Formal analysis, Resources, Data curation, Investigation, Resources, Writing - original draft, Writing - review & editing, Visualization, Funding acquisition. Eriberto Oliveira do Nascimento: Conceptualization, Methodology, Validation, Formal analysis, Resources, Validation Methodology, Software, Formal analysis, Data curation, Writing - review & editing. Pedro de Aquino Morais Júnior: Conceptualization, Methodology, Validation, Formal analysis, Resources, Data curation, Investigation. Patrícia de Lara Antonio: Conceptualization, Methodology, Validation, Formal analysis, Resources, Data curation, Investigation, Resources. Linda V.E. Caldas: Methodology, Supervision, Writing - review & editing, Funding acquisition

Declaration of competing interest

The authors declare that they have no known competing financial interests or personal relationships that could have appeared to influence the work reported in this paper.

Acknowledgments

The authors thank the Brazilian funding agency CNPq (Projects 104486/2019–8, 151945/2019–5 and 301335/2016–8) and FAPESP (Project 2018/05982–0) for partial financial support.

References

Bachmann, L., Diebolder, R., Hibst, R., Zezell, D.M., 2003. Infrared absorption bands of enamel and dentin tissues from human and bovine teeth. Appl. Spectrosc. Rev. 38, 1–14. https://doi.org/10.1081/ASR-120017479.

Baker, M.J., Trevisan, J., Bassan, P., Bhargava, R., Butler, H.J., Dorling, K.M., Fielden, P. R., Fogarty, S.W., Fullwood, N.J., Heys, K.A., Hughes, C., Lasch, P., Martin-Hirsch, P. L., Obinaju, B., Sockalingum, G.D., Sulé-Suso, J., Strong, R.J., Walsh, M.J., Wood, B. R., Gardner, P., Martin, F.L., 2014. Using Fourier transform IR spectroscopy to analyze biological materials. Nat. Protoc. 9, 1771–1791. https://doi.org/10.1038/nprot.2014.110.

Bargh, S., Silindir-Gunay, M., Ozer, A.Y., Palaska, E., Karaarslan, D., Ide, S., Solpan, D., 2020. Physicochemical evaluation of gamma and microwave irradiated dental grafts. Radiat. Phys. Chem. 170, 108627. https://doi.org/10.1016/j.radphyschem.2019.108627.

Bayarı, S.H., Özdemir, K., Sen, E.H., Araujo-Andrade, C., Erdal, Y.S., 2020. Application of ATR-FTIR spectroscopy and chemometrics for the discrimination of human bone remains from different archaeological sites in Turkey. Spectrochim. Acta Mol. Biomol. Spectrosc. 237, 118311. https://doi.org/10.1016/J.SAA.2020.118311.

Bertrand, D., Qannari, E.M., Vigneau, E., 2001. Latent root regression analysis: an alternative method to PLS. Chemometr. Intell. Lab. Syst. 58, 227–234. https://doi.org/10.1016/S0169-7439(01)00161-7.

Bonet, M., García, V., Farré, N., Algara, M., Farrús, B., Fernandez, J., Reyes, V., Eraso, A., Álvarez, A., Cambra, M.J., Pedro, A., Vayreda, J., Lemansky, C., Izar, F., Arenas, M., 2020. Radiation therapy for bone-only metastases in breast cancer patients: a GOCO survey of current clinical practice. Rep. Practical Oncol. Radiother. 25, 113–116. https://doi.org/10.1016/j.rpor.2019.12.019.

Chaber, R., Łach, K., Depciuch, J., Szmuc, K., Michalak, E., Raciborska, A., Koziorowska, A., Cebulski, J., 2017. Fourier Transform Infrared (FTIR) spectroscopy of paraffin and deparafinnized bone tissue samples as a diagnostic tool for Ewing sarcoma of bones. Infrared Phys. Technol. 85, 364–371. https://doi.org/10.1016/J.INFRARED.2017.07.017.

Das, B., Manohara, K.K., Mahajan, G.R., Sahoo, R.N., 2020. Spectroscopy based novel spectral indices, PCA- and PLSR-coupled machine learning models for salinity stress phenotyping of rice. Spectrochim. Acta Mol. Biomol. Spectrosc. 229 https://doi.org/10.1016/j.saa.2019.117983.

de Oliveira, L.N., de Almeida, A., Caldas, L.V.E., 2014. Fricke gel diffusion coefficient measurements for applications in radiotherapy level dosimetry. Radiat. Phys. Chem. 98, 42–45. https://doi.org/10.1016/J.RADPHYSCHEM.2014.01.008.

de Oliveira, L.N., do Nascimento, E.O., Andreeta, M.R.B., Antonio, P.L., Caldas, L.V.E., 2019. Characterization of lithium diborate, sodium diborate and commercial soda-lime glass exposed to gamma radiation via linearity analyses. Radiat. Phys. Chem. 155, 133–137. https://doi.org/10.1016/j.radphyschem.2018.06.031.

Donnelly, E., Meredith, D.S., Nguyen, J.T., Boskey, A.L., 2012. Bone tissue composition varies across anatomic sites in the proximal femur and the iliac crest. J. Orthop. Res. 30, 700–706. https://doi.org/10.1002/jor.21574.

dos Santos, F.R., de Oliveira, J.F., Bona, E., dos Santos, J.V.F., Barboza, G.M.C., Melquiades, F.L., 2020. EDXRF spectral data combined with PLSR to determine some soil fertility indicators. Microchem. J. 152 https://doi.org/10.1016/j.microc.2019.104275.

Drost, L., Ganesh, V., Wan, B.A., Raman, S., Chan, S., Christakis, M., Tsao, M., Barnes, E., Ford, M., Finkelstein, J., Yee, A., Turner, A., Lam, H., Chow, E., 2017. Efficacy of postoperative radiation treatment for bone metastases in the extremities. Radiother. Oncol. 124, 45–48. https://doi.org/10.1016/j.radonc.2017.05.010.

Govey, P.M., Zhang, Y., Donahue, H.J., 2016. Mechanical loading attenuates radiation-induced bone loss in bone marrow transplanted mice. PloS One 11, 167673. https://doi.org/10.1371/journal.pone.0167673.

Harig, R., 2004. Passive remote sensing of pollutant clouds by Fourier-transform infrared spectrometry: signal-to-noise ratio as a function of spectral resolution. Appl. Optic. 43, 4603–4610. https://doi.org/10.1364/AO.43.004603.

Helland, I.S., 2001. Some theoretical aspects of partial least squares regression. Chemometr. Intell. Lab. Syst. 58, 97–107. https://doi.org/10.1016/S0169-7439(01)00154-X.

Jiang, H., Lu, J., 2018. Using an optimal CC-PLSR-RBFNN model and NIR spectroscopy for the starch content determination in corn. Spectrochim. Acta Mol. Biomol. Spectrosc. 196, 131–140. https://doi.org/10.1016/j.saa.2018.02.017.

Kazakis, N.A., Tsirliganis, N.C., 2019. Optically stimulated luminescence investigation of chicken bones towards their use at food post-sterilization and retrospective dosimetry. Appl. Radiat. Isot. 154, 108899. https://doi.org/10.1016/j.apradiso.2019.108899.

Khanarian, N.T., Boushell, M.K., Spalazzi, J.P., Pleshko, N., Boskey, A.L., Lu, H.H., 2014. FTIR-I compositional mapping of the cartilage-to-bone interface as a function of tissue region and age. J. Bone Miner. Res. 29, 2643–2652. https://doi.org/10.1002/jbmr.2284.

Kontopoulos, I., Presslee, S., Penkman, K., Collins, M.J., 2018. Preparation of bone powder for FTIR-ATR analysis: the particle size effect. Vib. Spectrosc. 99, 167–177. https://doi.org/10.1016/J.VIBSPEC.2018.09.004.

Kubisz, L., Połomska, M., 2007. FT NIR Raman studies on γ-irradiated bone. Spectrochim. Acta Mol. Biomol. Spectrosc. 66, 616–625. https://doi.org/10.1016/J.SAA.2006.04.003.

Li, C.Q., Fang, Z., Xu, Q.S., 2020. A partition-based variable selection in partial least squares regression. Chemometr. Intell. Lab. Syst. 198, 103935. https://doi.org/10.1016/j.chemolab.2020.103935.

Lu, C.C., Wang, F.N., Lin, H.H., Hsu, C.H., Lin, J.P., Lai, L.H., 2020. Dosimetric measurement of testicular dose for colorectal cancer using optically-stimulated luminescent dosimeters in radiotherapy. Radiat. Phys. Chem. 172, 108792. https://doi.org/10.1016/j.radphyschem.2020.108792.

Luinge, H.J., van der Maas, J.H., Visser, T., 1995. Partial least squares regression as a multivariate tool for the interpretation of infrared spectra. Chemometr. Intell. Lab. Syst. 28, 129–138. https://doi.org/10.1016/0169-7439(95)80045-B.

Mandair, G.S., Oest, M.E., Mann, K.A., Morris, M.D., Damron, T.A., Kohn, D.H., 2020. Radiation-induced changes to bone composition extend beyond periosteal bone. BoneKEy Rep. 12 https://doi.org/10.1016/j.bonr.2020.100262.

Musto, E., Assenmacher, F., Hofstetter-Boillat, B., Mayer, S., Yukihara, E.G., 2019. Use of the D-Shuttle dosimeter for radiation protection of members of the public: characterization and feasibility study. Radiat. Meas. 129, 106208. https://doi.org/10.1016/j.radmeas.2019.106208.

Parwaie, W., Geraily, G., Shirazi, A., Shakeri, A., Massumi, H., farzin, M., 2020. Analysis of the ferrous benzoic methylthymol-blue gel dosimeter in low-dose-level measurements. Radiat. Phys. Chem. 173, 108943. https://doi.org/10.1016/j.radphyschem.2020.108943.

Petra, M., Anastassopoulou, J., Theologis, T., Theophanides, T., 2005. Synchrotron micro-FT-IR spectroscopic evaluation of normal paediatric human bone. J. Mol. Struct. 733, 101–110. https://doi.org/10.1016/j.molstruc.2004.07.041.

Polanek, R., Varga, Z., Fodor, E., Brunner, S., Szabó, E.R., Tőkés, T., Hideghéty, K., 2020. Improved FBX chemical dosimeter system with enhanced radiochemical yield for reference dosimetry in radiobiology and radiotherapy research. Radiat. Phys. Chem. 174, 108899. https://doi.org/10.1016/j.radphyschem.2020.108899.

Rogalski, A., 2002. Infrared detectors: an overview. Infrared Phys. Technol. 43, 187–210. https://doi.org/10.1016/S1350-4495(02)00140-8.

Rudko, V.v., Vorona, I.P., Baran, N.P., Ishchenko, S.S., 2009. Thermally stimulated transformation of the EPR spectra in γ-irradiated bone tissue. Radiat. Meas. 44, 239–242. https://doi.org/10.1016/j.radmeas.2009.03.016.

Saleh, H.H., Sharaf, J.M., Abady, R.S., 2021. Gamma-ray buildup factor and radiation absorbed dose enhancement at tissue-bone interfaces. Appl. Radiat. Isot. 167, 109464. https://doi.org/10.1016/j.apradiso.2020.109464.

Shiloh, R., Krishnan, M., 2018. Radiation for treatment of painful bone metastases. Hematol. Oncol. Clin. N. Am. 32 (3), 459–468. https://doi.org/10.1016/j.hoc.2018.01.008.

Sung, N.Y., Choi, J. il, 2015. Enhanced release of bone morphogenetic proteins from demineralized bone matrix by gamma irradiation. Radiat. Phys. Chem. 111, 62–66. https://doi.org/10.1016/j.radphyschem.2015.02.012.

Tiplady, K.M., Sherlock, R.G., Littlejohn, M.D., Pryce, J.E., Davis, S.R., Garrick, D.J., Spelman, R.J., Harris, B.L., 2019. Strategies for noise reduction and standardization of milk mid-infrared spectra from dairy cattle. J. Dairy Sci. 102, 6357–6372. https://doi.org/10.3168/jds.2018-16144.

Urbański, P., 1994. Principal component and partial least squares regressions in the calibration of nucleonic gauges. Appl. Radiat. Isot. 45, 659–667. https://doi.org/10.1016/0969-8043(94)90244-5.

Wold, S., Sjöström, M., Eriksson, L., 2001. PLS-regression: a basic tool of chemometrics. Chemometr. Intell. Lab. Syst. 58, 109–130. https://doi.org/10.1016/S0169-7439(01)00155-1.

Zhang, H., Li, Z., Chen, T., Qin, B., 2017. Quantitative determination of Auramine O by terahertz spectroscopy with 2DCOS-PLSR model. Spectrochim. Acta Mol. Biomol. Spectrosc. 184, 335–341. https://doi.org/10.1016/j.saa.2017.05.017.